Using SCIAMACHY to improve corrections for spectral band differences when transferring calibration between visible sensors

Benjamin Scarino*[a], David R. Doelling[b], Daniel L. Morstad[a], Rajendra Bhatt[a], Arun Gopalan[a], Constantine Lukashin[b], Patrick Minnis[b]
[a]SSAI, One Enterprise Pkwy Ste 200, Hampton, VA 23666 USA
[b]NASA Langley Research Center, 21 Langley Blvd MS 420, Hampton, VA 23681-2199 USA

ABSTRACT

The advent of well-calibrated and well-characterized visible sensors, such as the MODerate resolution Imaging Spectroradiometer (MODIS), has allowed the opportunity to cross-calibrate other contemporary, un-calibrated visible sensors. Most of the operational geostationary-Earth-orbit satellite (GEOsat) visible sensors do not have a direct means of on-orbit calibration, and the cross-calibration of MODIS with GEOsats is plagued by the differences in the sensor spectral response functions (SRFs). Spectral band adjustment factors (SBAFs) are needed to correct for the solar flux and inter-band gaseous absorption discrepancies that are caused by SRF differences, which are sometimes significant. In addressing this problem, this manuscript describes a spectral band correction technique that employs Envisat SCanning Imaging Absorption spectroMeter for Atmospheric CartograpHY (SCIAMACHY) hyper-spectral radiances to derive pseudo-radiance, or equivalent-radiance, values for the MODIS and GEOsat sensors over the calibration targets, which include a desert, deep convective clouds, and a MODIS-with-GEOsat ray-matching ocean domain. The regressions from these equivalent-radiance comparisons constitute the necessary adjustment factor. The regressions of MODIS and GEOsat pseudo-radiance values are well-behaved, with small standard error and offsets, for spectral bands that are similar. When comparing narrowband to broadband, however, the correction difference between deep convective and maritime stratus clouds can be as large as 6%. New scene-selection criteria are investigated to derive spectral band adjustment factors that are dependent on the calibration-target domains, which reduces this uncertainty. Application of these SBAFs, which are validated for accuracy using ray-matched SCIAMACHY and GEOstat radiances, is shown to bring independently derived absolute calibrations to within 1% agreement, or better, with one-another. These spectral band adjustment factors are critical for obtaining accurate and consistent absolute calibration among multiple independent and scene-dependent inter-calibration techniques given that the variation of the SBAFs as a function of scene type can be close to 8% for a narrowband-to-broadband correction.

Keywords: SCIAMACHY, Meteosat, MODIS, radiometric calibration, hyper-spectral, spectral response function, spectral correction, ray-match, deep convective clouds, pseudo-invariant desert

1. INTRODUCTION

Hyper-spectral instruments are ideal for calibrating geostationary-Earth-orbit satellite (GEOsat) imagers because hyper-spectral radiances are well-calibrated and can account for spectral response function (SRF) differences[1,2,3,4]. The Global Space-Based Inter-Calibration System (GSICS) employs such hyper-spectral instrument radiances as a calibration reference to standardize GEOsat infrared imagers[5]. The same technique can be used to transfer the calibration of a contemporary, well-calibrated visible sensor, such as the MODerate resolution Imaging Spectroradiometer (MODIS), to a GEOsat, such as Meteosat-9 (Met-9), using Envisat SCanning Imaging Absorption spectroMeter for Atmospheric CartograpHY (SCIAMACHY) hyper-spectral radiances. The SCIAMACHY hyper-spectral radiances are useful in accounting for SRF differences and deriving scene-specific spectral corrections – steps that are necessary for developing absolute calibrations of visible imagers.

Depending on the width of the spectral bands one is comparing, the correction required to normalized one instrument to another can vary in significance. For example, the 0.65-μm channels (CH1) of MODIS and Met-9 are both narrowband, and therefore the correction is expected to be minimal. The SRF of the Met-9 broadband High Resolution Visible (HRV) channel, however, is rather wide compared to the MODIS CH1 SRF (Fig. 1). Thus, a larger correction is expected. The SCIAMACHY hyper-spectral radiances can be used to account for differences of nearly any significance,

*benjamin.r.scarino@nasa.gov; phone 1 757 951-1622; fax 1 757 951-1902

Earth Observing Systems XVII, edited by James J. Butler, Xiaoxiong Xiong, Xingfa Gu,
Proc. of SPIE Vol. 8510, 85100Q · © 2012 SPIE · CCC code: 0277-786X/12/$18 · doi: 10.1117/12.929767

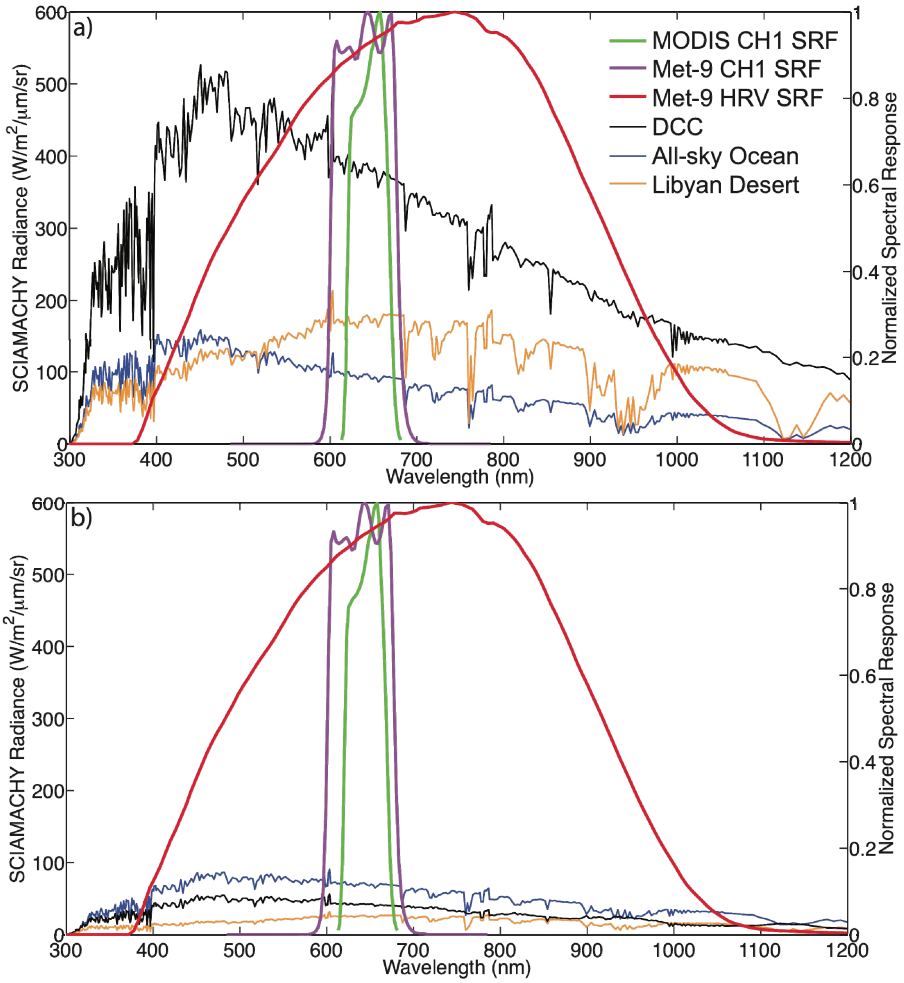

Figure 1. Spectral response functions of Aqua-MODIS CH1 (0.65 μm), Met-9 CH1 (0.65 μm), and Met-9 HRV relative to deep convective clouds (DCC), all-sky ocean, and Libyan desert **(a)** mean SCIAMACHY hyper-spectral radiance and associated **(b)** standard deviation measured from August 2002 through December 2010.

in most of the visible spectrum, through use of calibration-target-dependent spectral band adjustment factors (SBAFs). Performing the correction in terms of radiances allows for simultaneous correction for solar flux and inter-band gaseous absorption differences.

The aim of this manuscript is to demonstrate the effectiveness of the SCIAMACHY-based spectral radiance corrections in improving absolute calibrations for a GEOsat through three independent absolute calibration techniques – the MODIS-with-GEOsat ray-matching technique, the deep-convective-cloud (DCC) technique, and the pseudo-invariant desert site technique. The calibration accuracy of SCIAMACHY is assessed using Aqua-MODIS as a standard. Additionally, the importance of scene-selection when developing SCIAMACHY-based SBAFs is demonstrated with a narrowband-to-broadband comparison. Ultimately, the results will indicate an overall improved agreement in the absolute calibrations found from the three independent methods when the spectral corrections are applied. Comparisons with direct ray-matched SCIAMACHY and GEOsat radiances are used to assess the accuracy of the method.

2. DATA AND METHODOLOGY

Although SCIAMACHY-based spectral band difference corrections have been used for transferring calibrations between many visible sensors over several GEOsat equatorial domains, this manuscript focuses on the correction for differences between MODIS and Met-9.

2.1 SCIAMACHY specifications

The SCIAMACHY instrument is onboard the European Space Agency Environmental Satellite (Envisat), which was launched on 1 March 2002 into a 10:00 AM Local Stand Time (LST) sun-synchronous orbit, with a mean altitude of 800 km and a 35-day repeat cycle. This study employs SCIAMACHY Level-1b, Version-7.03 radiances from 2002 through 2010. At 1-sec integration time, SCIAMACHY has a spatial resolution of 30-km along-track by 240-km across-track for the nadir-like scans, which alternate evenly with limb scans every 7 minutes[6]. There are two nadir-like footprints on each side of the ground track within a 30° view angle (two interior near-nadir, and two exterior far-nadir footprints), resulting in a total nadir scan width of 960 km. The SCIAMACHY instrument has 8 channels covering 240 – 2380 nm, with a majority of the visible spectrum passing to channels 3 – 6 (394 – 1750 nm) at a spectral resolution of 0.44 – 1.48 nm[6,7,8]. Direct sun measurements are used operationally for degradation monitoring, which can also be checked with moon observations. The SCIAMACHY absolute on-orbit calibration reflectance accuracies for channels 4 and 5 (604 – 805 nm and 785 – 1050 nm) are 2% and 6%, respectively, and the channel 3 and 6 accuracies are between that range[9].

2.2 SCIAMACHY-based spectral band adjustment factors

The method of calculating the SBAFs for the visible sensors is similar to that of Doelling et al.[10]. To normalize the calibration of one imager to another, SCIAMACHY footprints were taken from August 2002 through December 2010 in the Met-9 sub-satellite equatorial domain (15.0°S to 15.0°N, and 20.0°W to 20.0°E) for DCC and ocean scenes and over the Libyan Desert (28.0°N to 29.5°N, and 22.5°E to 24.0°E). The spectra from each SCIAMACHY pixel were then convolved with the Aqua-MODIS CH1 and Met-9 CH1 and HRV SRFs to compute imager equivalent radiances. A regression of the two convolved SCIAMACHY radiances constitutes a radiance-dependent SBAF that should be applied to the reference sensor radiance to arrive at the predicted target sensor radiance.

Land use is determined by International Geosphere-Biosphere Programme (IGBP) land classification, and cloud properties are determined by matching the SCIAMACHY pixels with the Clouds and the Earth's Radiant Energy System (CERES) Single Scanner Footprint (SSF) and associated MODIS cloud retrievals taken approximately half an hour after the Envisat overpass[11]. The criteria for a DCC footprint are as follows: The cloud fraction at the center of the SCIAMACHY footprint must be greater than 99%, the cloud top temperature must be below 205 K, the cloud optical depth must be between 70 and 150, and the solar zenith angle (SZA) must be less than 45°. For all-sky ocean scenes (applicable for the narrowband), the four corners and center of the footprint must register as at least 90% ocean. Owing to the broadband nature of the Met-9 HRV channel, footprints containing DCC and high clouds must be separated from the clear-sky and low-cloud (marine stratus) footprints. Thus, the only SCIAMACHY footprints used for this band are ones where the cloud fractions at the four corners and center are less than 1%, or the entire footprint is cloudy with a cloud top temperature greater than 270 K. The Libyan Desert SBAFs use only clear scenes, which are determined by a spatial standard deviation threshold using Met-7 (before 2007) or Met-9 pixels[12].

2.3 Ray-matching- DCC- and desert-based absolute calibration methods

The three independent calibration methodologies described in this section follow closely to those described by Morstad et al.[13] and Bhatt et al.[14], but will be restated here in brief. First, the ray-matching inter-calibration technique employs co-incident, co-angled, and co-located ocean region pixels imaged by the Aqua-MODIS and Met-9 sensors[13,15,16]. The Met-9 imager 10-bit counts, which are proportional to radiance, are calibrated against Aqua-MODIS using monthly regressed ray-matched radiance pairs over the Met-9 equatorial domain. The 10-bit counts, C, are converted to radiance, L, by applying the absolute gain of the sensor, which is the slope of the monthly regression forced through the space count, or count offset, of Met-9 (equal to 51). The monthly gains are linearly regressed in time to monitor the Met-9 instrument degradation. Thus, Met-9 counts are converted to radiance via

$$L_{ref} \times SBAF_{tar/ref} = L_{tar} = \left(\Delta g_1 \times DSL + g_o\right)\left(C - C_o\right), \quad (1)$$

where g_o is the initial gain, Δg_1 is the linear term of the trend, DSL is the days since launch (21 December 2005) of Met-9, and C_o is the space count[13,17]. An ocean-based SBAF is applied to the MODIS reference radiances (L_{ref}) to account for SRF differences and arrive at the predicted Met-9 target radiances (L_{tar}). Second, the deep-convective-cloud inter-calibration technique assumes the constancy of the DCC broadband albedo response can be used to verify the stability of two imagers[13,18,19,20]. This predictability is evident from the low standard deviation of the DCC spectra (Fig. 1b). The generalized approach uses DCC as invariant earth targets, with the Aqua-MODIS calibration transfer dependent on matched DCC targets between MODIS and the GEOsat[13]. A DCC-based SBAF accounts for the SRF differences.

Finally, the desert-based absolute calibration technique follows the base assumption that radiance from certain ground sites, in this case the Libyan Desert, is constant over time (Fig. 1b)[12,13,14]. The method employs a kernel-based bidirectional reflectance distribution function (BRDF) model developed using ten years of calibrated Aqua-MODIS radiances. An SBAF is applied to the BRDF model output in order to arrive at a correct predicted top-of-atmosphere radiance for Met-9.

2.4 SCIAMACHY nearly simultaneous nadir overpass calibration with Aqua-MODIS

Before being used to account for spectral band differences, it is important to verify the calibration of SCIAMACHY. The MODIS-with-GEOsat ray-matching, DCC, and desert calibration transfer techniques discussed in this study use Aqua-MODIS as the calibration reference. Aqua-MODIS is chosen following recommendations from the GSICS community, and because Aqua-MODIS is a better-characterized, more-temporally-stable instrument compared to Terra-MODIS[21]. To radiometrically scale the SCIAMACHY radiances to Aqua-MODIS CH1, nearly simultaneous nadir overpass (NSNO) measurements are compared. The NSNO comparisons are conducted using Aqua-MODIS Collection-6, Level-1b CH1 pixel-level radiances, which have a 1-km nominal resolution, but were sub-sampled at 2 km. The absolute calibration accuracy of Aqua-MODIS CH1, in reflectance, is ~2%[22], and is estimated to be stable within 0.5% per decade[21].

The SCIAMACHY/Aqua-MODIS NSNO inter-calibration methodology is described by Doelling et al.[17]. About 60 NSNO matches near 70°N are captured monthly, with that amount limited by the SCIAMACHY limb/nadir duty cycle and SZA considerations. Only matches for which the SZA is less than 70° are used in order to maintain an acceptable signal-to-noise ratio. As a result, the comparison is limited to the April through September months. The NSNOs occur 14 times daily at ~11:45 AM LST, thereby assuring near-symmetric solar conditions. Figure 2 illustrates the orientation of the SCIAMACHY footprint relative to the satellite ground tracks during one of these overpasses. Only the southern near-nadir SCIAMACHY footprint is used. Within the bounds of this footprint, the MODIS 2-km pixel-level radiances are averaged, normalized to the SZA of the SCIAMACHY footprint, and, on a monthly basis, regressed with SCIAMACHY radiance values that are convolved with the MODIS CH1 SRF (Fig. 3). The force-fit regression through the origin, which represents the ratio of the means of each instrument, is used as the monthly correction factor. Regressions are also performed on a three-monthly basis, and, for this manuscript, on a yearly bases.

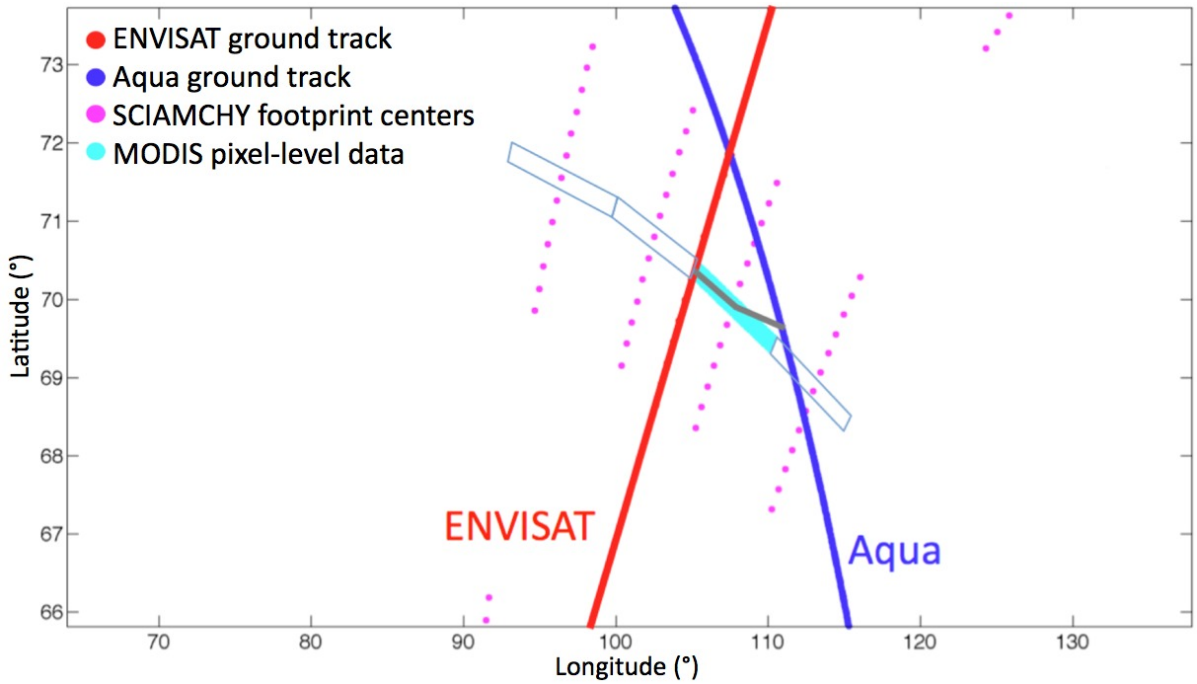

Figure 2. SCIAMACHY footprint centers and accompanying Envisat and Aqua ground tracks. The thin rectangles identify the four SCIAMACHY footprints that constitute the 960-km cross-track swath. The thick gray lines show the cross-track orientation of the SCIAMACHY footprint and Aqua-MODIS pixels.

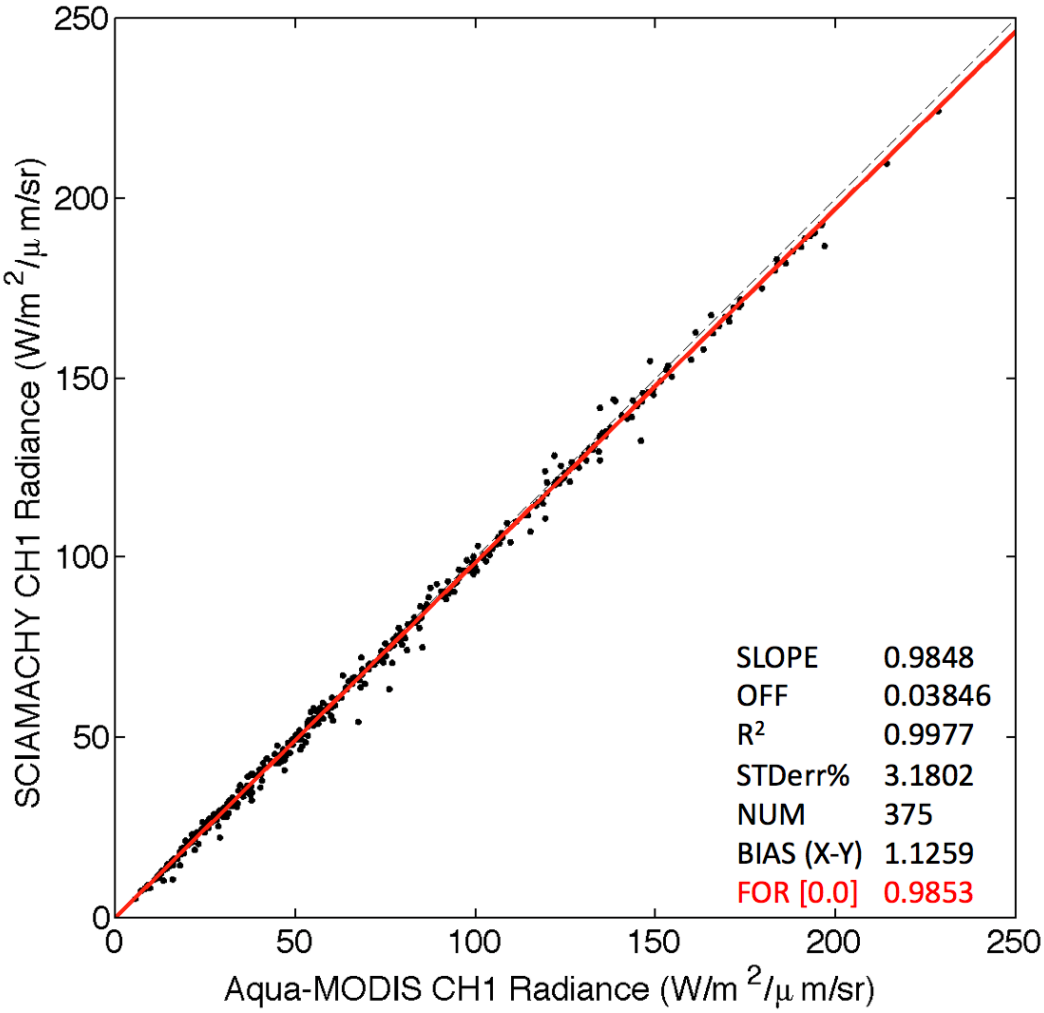

Figure 3. Nearly simultaneous nadir overpass match comparisons of Aqua-MODIS Collection-6 CH1 radiances and SCIAMACHY radiances convolved with the Aqua-MODIS CH1 SRF for April – September 2004.

2.5 SCIAMACHY/GEOsat ray-matching inter-calibration

In order to accurately compare SCIAMACHY with a GEOsat, the viewing zenith angle (VZA) of the GEOsat must match the VZA at the center of the SCIAMACHY footprint[17]. In this study, this ray-matching, or bore-sighting, method is possible at only four locations for each GEOsat. The four ray-matched locations of the Met-9 domain are illustrated in Fig. 4, with each location specific to one of the four cross-track SCIAMACHY footprints, each of which has a unique VZA. That is, the east-most (west-most) ray-matched location corresponds to the east-most (west-most) SCIAMACHY footprint (see Fig. 4). Any time the appropriate SCIAMACHY footprint center is within 160 km of its match location, an average radiance is computed using the GEOsat 4-km pixel 10-bit counts inside the bounds of the SCIAMACHY footprint, provided that the pixels were scanned within 15 minutes of the SCIAMACHY overpass. Before they are averaged, the GEOsat 10-bit counts are converted to spectral radiance following Eq. 1. This radiance average is then compared to the corresponding SCIAMACHY footprint hyper-spectral radiance convolved with the GEOsat SRF (Met-9 CH1 and HRV; Fig. 1). Given that the GEOsat imager counts were first calibrated against Aqua-MODIS (Eq. 1), the SCIAMACHY radiances are first scaled to the Aqua-MODIS reference calibration (see Section 2.4). Figure 5 shows an example 3-month regression of Met-9 CH1 and convolved SCIAMACHY matched radiances. Considering the 35-day Envisat orbit repeat cycle, as well as the alternating scan duty, a ray-match comparison occurs roughly 50 times each month, which is enough to resolve the temporal degradation of the GEOsat visible sensor. An inherent benefit of this method is that near-exact solar and azimuthal geometry matching is ensured given that the line that defines the cross-track intersects the GEOsat sub-satellite point.

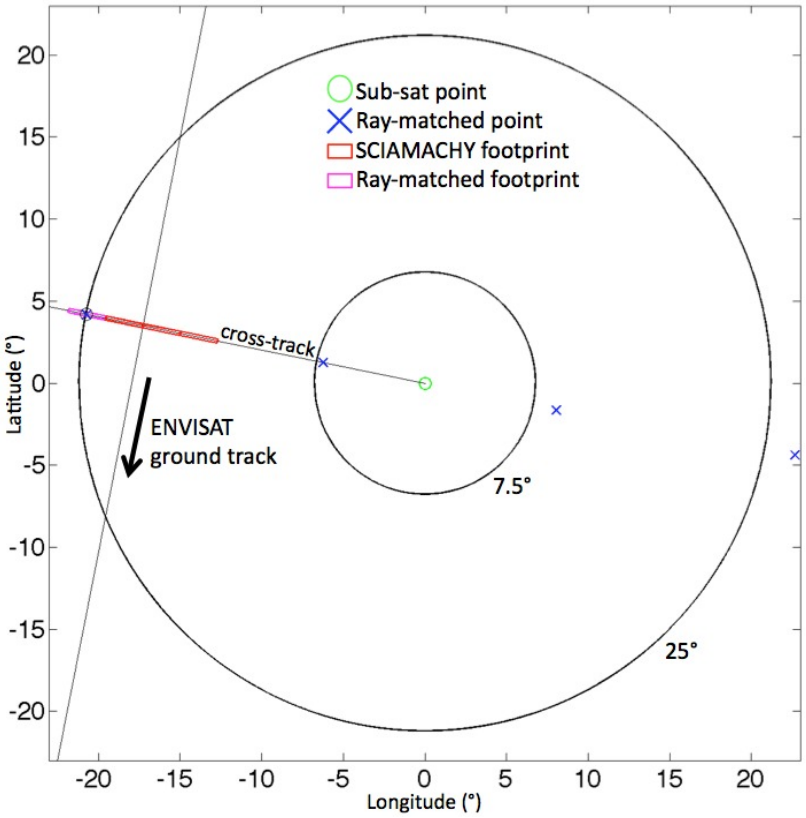

Figure 4. The orientation of the four ray-matched locations associated with Met-9. The inner (outer) circle demarcates the 7.5° (25°) view angle of Met-9.

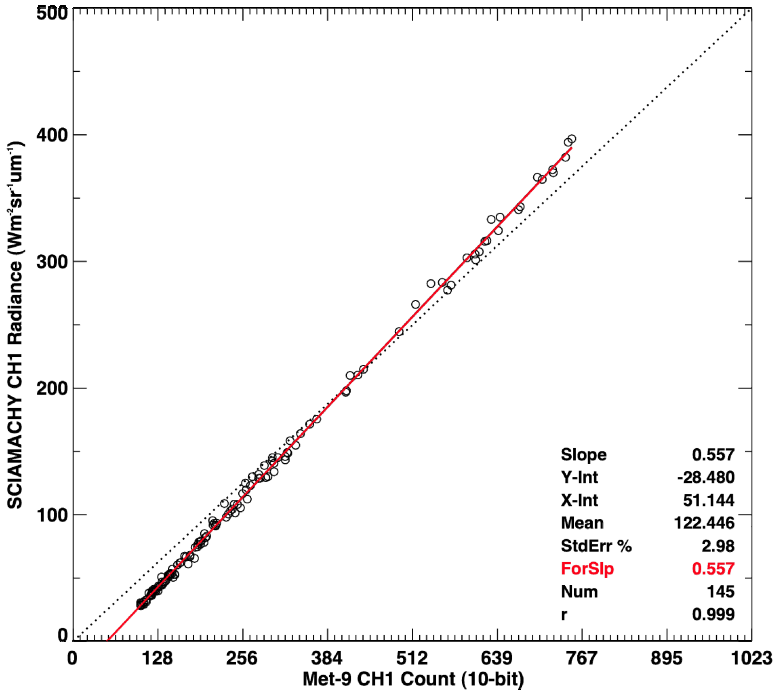

Figure 5. Ray-matched comparisons of Met-9 CH1 10-bit counts and SCIAMACHY radiance convolved with the Met-9 CH1 SRF for January – March 2008.

3. RESULTS AND DISCUSSION

3.1 SCIAMACHY narrowband and broadband spectral corrections

Regressions of SCIAMACHY radiances convolved with the Aqua-MODIS CH1 and Met-9 CH1 SRFs are shown for DCC, all-sky ocean, and Libyan Desert in Fig. 6. The type of regression used for the SBAF should consistently be the best fit for the entire dynamic range the data. For DCC and desert scenes (Figs. 6b and 6c), a linear regression forced through the origin is used as the SBAF. For ocean ray-matching scenes (Fig. 6a), a first-order regression is the more consistent choice, however, a second-order regression is used instead owing to a slight improvement in standard error.

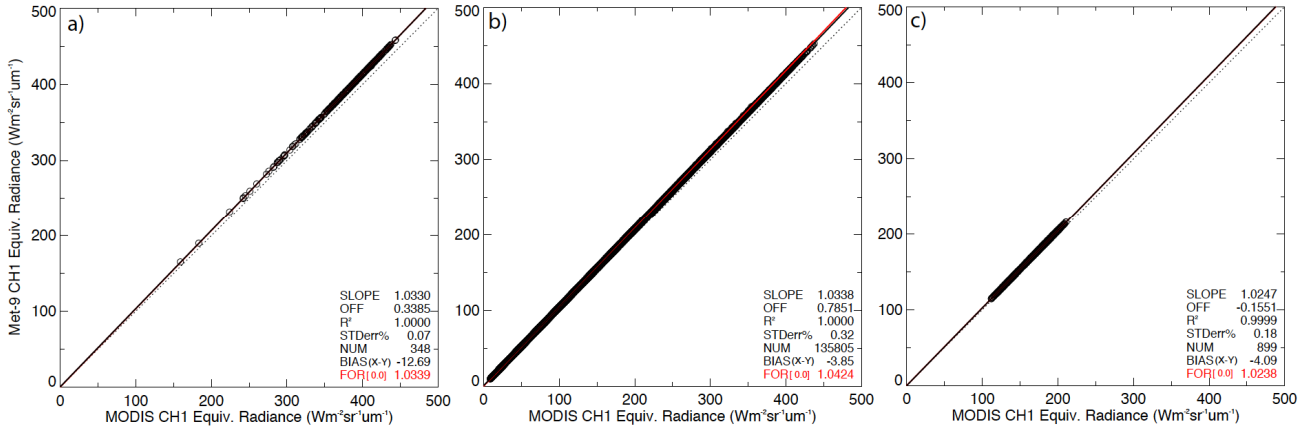

Figure 6. Regressions of SCIAMACHY radiances convolved with Aqua-MODIS and Met-9 CH1 SRFs for **(a)** DCC, **(b)** all-sky ocean (ray-matching), **(c)** and Libyan Desert scenes. Second-order fit for the all-sky ocean regression not shown.

Figure 7 shows regressions of SCIAMACHY radiances convolved with the Aqua-MODIS CH1 and Met-9 HRV SRFs. For a narrowband-to-broadband case such as this, for which there is no unique relationship between narrowband-to-broadband radiances, there is no type of regression that can sufficiently resolve the SBAF functionality (Fig. 7a). This outcome suggests that multiple SBAFs, based on varied cloud types, are necessary. Thereby, the information in Fig. 7a is divided into either a DCC or marine-stratus category (Figs. 7b and 7c) in order to yield unique, scene-specific SBAFs. When the DCC clouds (Fig. 7b) are separated, using conditions set in Section 2.2, from the marine stratus clouds and clear-ocean scenes (Fig. 7c), a regression can adequately provide distinct SBAFs for use in the DCC and Aqua-MODIS-with-Met-9-HRV ray-matching inter-calibration schemes. Isolating the clear-sky and marine stratus from the DCC is necessary given the potential ~6% SBAF variance in the all-sky ocean case (Fig. 7a), which is the difference in the slopes encompassing the distribution of radiances pairs. Similarly, marine stratus clouds are used for the Aqua-MODIS-CH1-with-Met-9-HRV ray-matching inter-calibration method. All IR pixels with a brightness temperature greater than 270 K, and radiance values less than 100 $Wm^{-2}sr^{-1}\mu m^{-1}$, are used to isolate marine stratus and clear-sky conditions. For this HRV ray-matching technique, only months that have a statistically significant number of marine stratus cases are used, which are typically the summer months of June through August. Finally, for the Met-9 HRV Libyan Desert inter-calibration scheme (Fig. 7d), four SBAFs are necessary to account for inter-seasonal variations in water vapor absorption over the desert.

Based on the SCIAMACHY MODIS CH1 and Met-9 HRV SRF-convolved radiance pairs, the first-order slopes for the DCC (Fig 7b), marine stratus (Fig 7c), and desert scenes (Fig 7d) are 0.896, 0.873, and 0.823, respectively. The solar constant ratio (see Section 3.2) is 0.883, suggesting that the atmosphere above the desert and marine stratus scenes reduces reflectance, relative to MODIS CH1, in the near-IR spectrum of the HRV channel. The reason for this reduction, and the reason why reflectance is not reduced for the DCC scenes, is because the near-IR wavelengths are strongly influenced by water vapor absorption. At the tropopause, where the DCC tops exist, there is little water vapor, and, thereby, little related absorption in the atmospheric column above the DCC. Therefore, for the DCC case, water vapor absorption has little influence in both the MODIS CH1 and Met-9 HRV bands. For the other, lower-troposphere cases, the Met-9 HRV channel is more influenced by water vapor absorption, thus the reflectance is reduced for these scenes. Comparatively, ozone is above the tropopause. Therefore ozone absorption, which is dominant at shorter wavelengths, does not change depending on scene type.

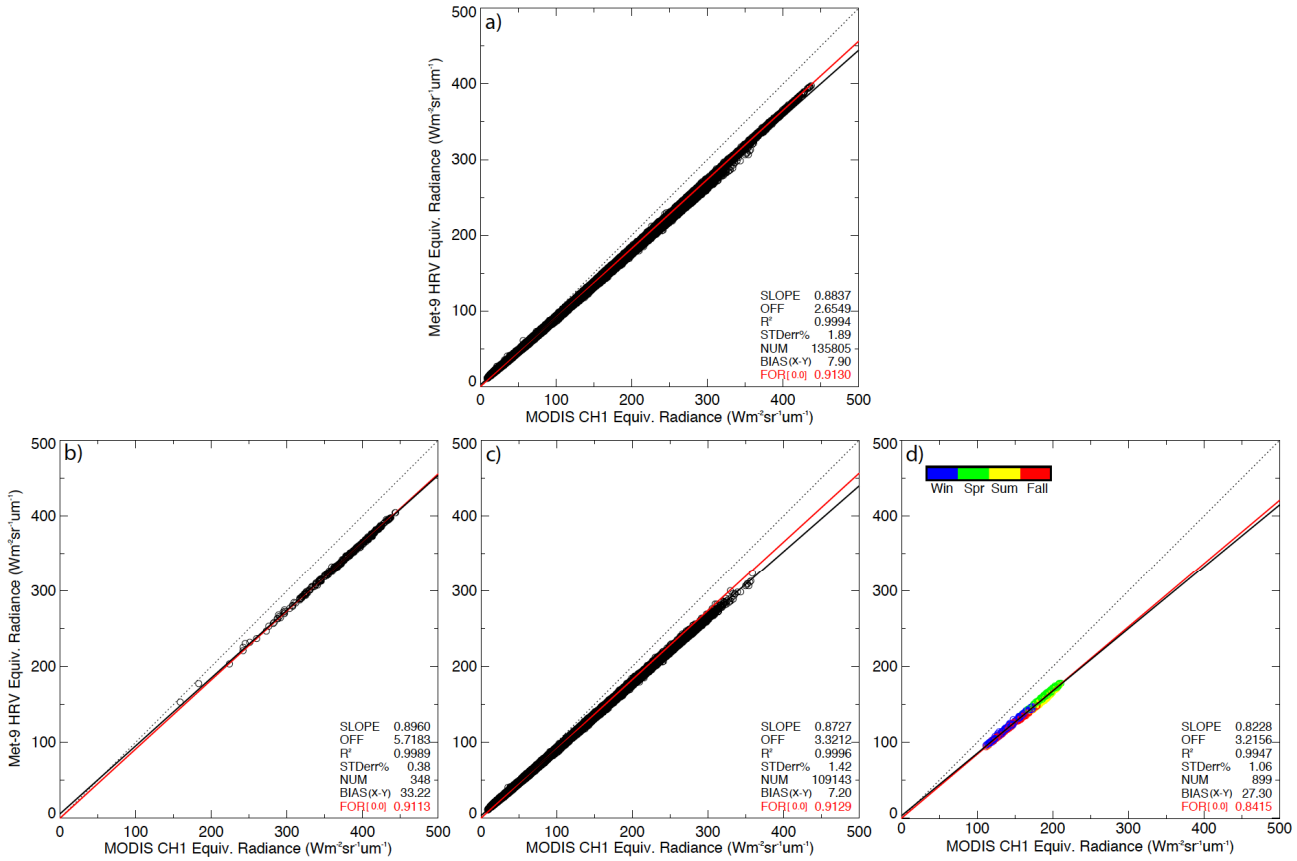

Figure 7. Regressions of SCIAMACHY radiances convolved with Aqua-MODIS CH1 and Met-9 HRV SRFs for **(a)** all-sky ocean (not used), **(b)** DCC, **(c)** marine stratus and clear ocean (ray-matching), **(d)** and Libyan Desert scenes. Second-order fit for the marine stratus and clear ocean regression not shown.

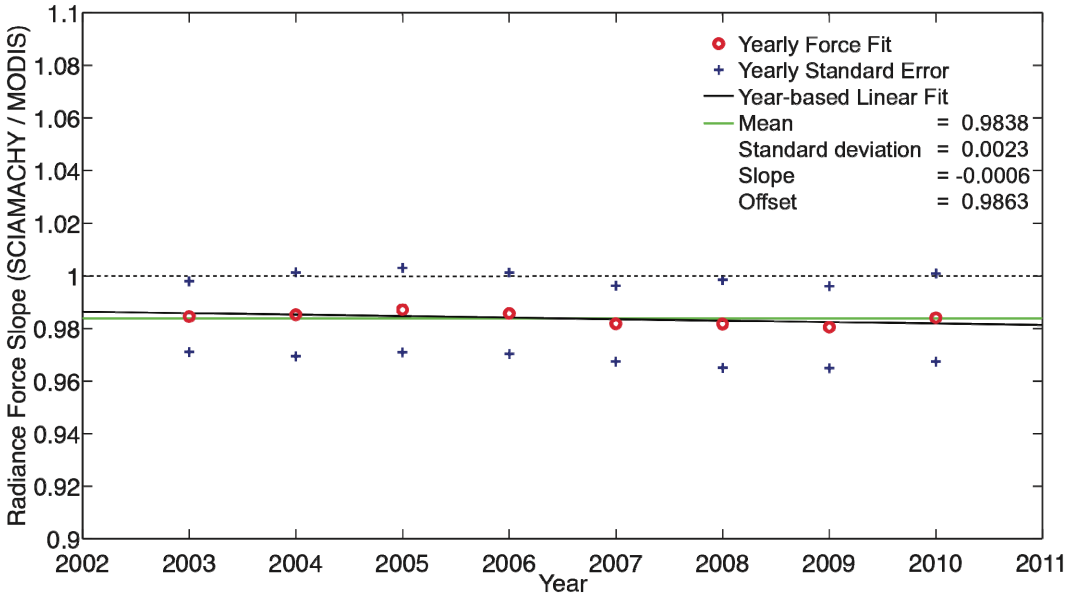

Figure 8. Yearly SCIAMACHY-to-Aqua-MODIS radiometric scaling factors from 2003 through 2010. The data from each year are treated as a whole and discreet point, with each point centered on 15 June of the indicated year. The standard error is plotted about the force fit.

3.2 SCIAMACHY-with-Aqua-MODIS NSNO and ray-matching findings

It is important to first establish the stability and accuracy of the SCIAMACHY sensor relative to a well-characterized instrument. A yearly timeline of SCIAMACHY-to-Aqua-MODIS correction factors, e.g., 0.9853 for 2004 from Fig. 3, is shown in Fig. 8. There is a mean correction value between SCIAMACHY and Aqua-MODIS of 0.9838, indicating that SCIAMACHY calibration is 1.6% darker than Aqua-MODIS in the CH1 band on average. The degradation of SCIAMACHY relative to Aqua-MODIS is 0.06% per year. This degradation and the 0.23% standard deviation indicate that both Aqua-MODIS and SCIAMACHY are rather stable.

Because the conversion from Met-9 10-bit counts to radiances uses coefficients based on MODIS ray-matching, the SCIAMACHY radiances used in the SCIAMACHY-with-Met-9 three-monthly regressions (Fig. 5) need to be adjusted by the SCIAMACHY-to-Aqua-MODIS mean radiometric scaling factor in order to yield an accurate gain. The 0.557 gain from Fig. 5 is therefore divided by the 0.9838 SCIAMACHY-to-Aqua-MODIS correction, resulting in a new gain of 0.566 for the January – March 2008 period. The corrected SCIAMACHY-with-Met-9 gains are plotted against the days since the launch of Met-9 in Fig. 9. The mean gain is 0.558, with a standard error of only 0.52%, meaning the data fit well to the linear trend.

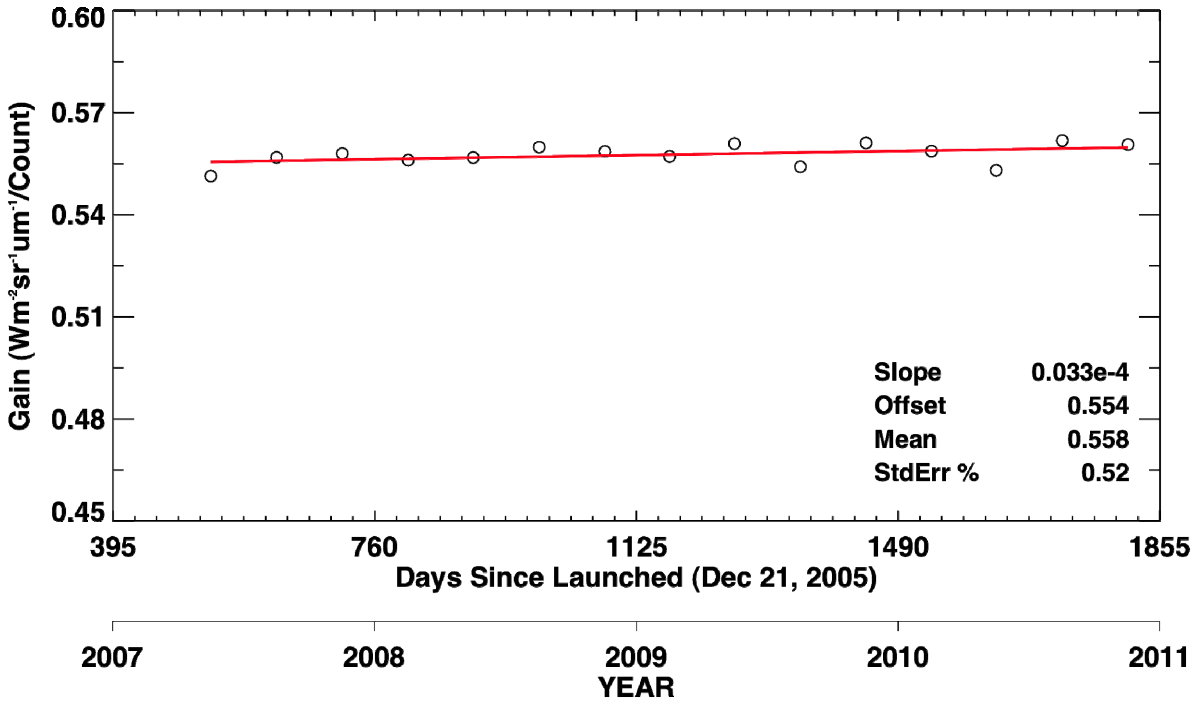

Figure 9. Three-monthly SCIAMACHY-with-Met-9 CH1 gains from April 2007 through December 2010.

3.3 Before and after application of SBAFs

The significance of SCIAMACHY-based spectral difference corrections is demonstrated with Figs. 10 and 11. These figures show the gains derived from the MODIS-with-Met-9 ray-matching, DCC, and Libyan Desert independent inter-calibration methods for Met-9 CH1 (Fig. 10) and the HRV channel (Fig. 11) before and after application of the SBAF. Before the SBAF is applied (Figs. 10a and 11a), the maximum mean difference in absolute calibration between the three methods for Met-9 CH1 and the HRV channel is 0.4% and 8.3%, respectively. After the SBAF is applied (Figs. 10b and 11b), the difference for Met-9 CH1 and the HRV channel reduces to within 0.2% and 1.0%, respectively. The mean difference in CH1 (HRV) gains, on average, from before to after application of the SBAF is +2.0% (-11.3%). In all cases, the standard error is near 1 – 2 %, indicating good representation of the data by the trend lines, for which the slope differences are within 0.0006%. These improvements demonstrate the importance of spectral difference corrections, and show that SCIAMACHY convolved hyper-spectral radiances can more-than-adequately account for both narrowband-to-narrowband and narrowband-to-broadband discrepancies.

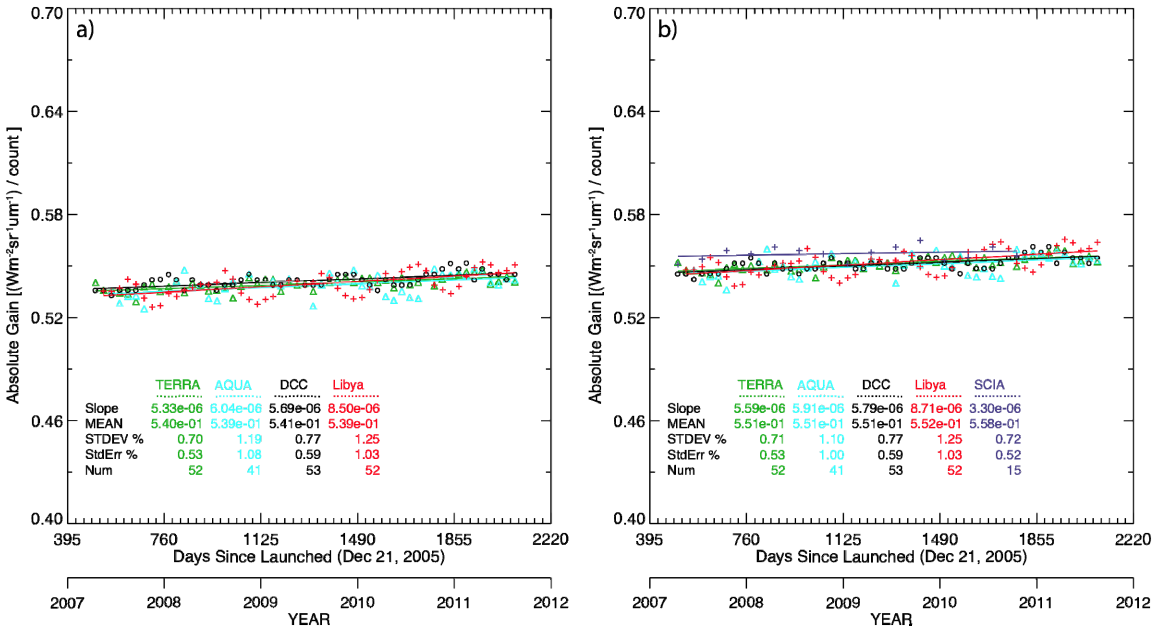

Figure 10. For Met-9 CH1, the MODIS-with-Met-9 ray-matching, DCC, Libyan Desert, and **(b only)** SCIAMACHY-with-Met-9 absolute calibrations **(a)** before and **(b)** after application of the SBAF.

The dark blue crosses and regression lines on Figs. 10b and 11b represent the three-monthly SCIAMACHY-with-Met-9 gains (Fig. 9). Results from this fourth independent calibration method (see Section 2.5) are plotted with the MODIS ray-matching, DCC, and Libyan Desert gains to validate the accuracy of SCIAMACHY-derived SBAFs. The SCIAMACHY ray-matching absolute calibration mean for Met-9 CH1 (HRV) is, on average, within 1.3% (0.2%) of that from the other methods after the SBAF is applied. The standard errors are well within 1%. Because this method's results are close to those of the other three calibration methods, and owing to fact that the SCIAMACHY-with-Met-9 ray-matching comparisons require no spectral correction, one can be confident that the SBAFs used to correct for spectral differences in the independent absolute calibrations are reasonably accurate.

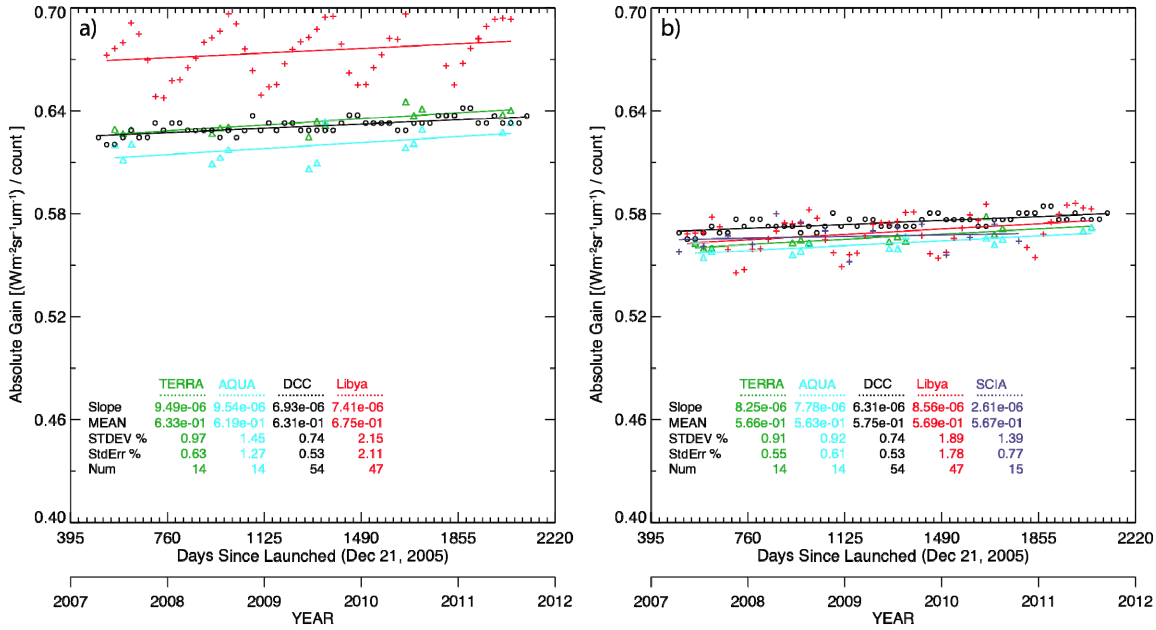

Figure 11. For the Met-9 HRV channel, the MODIS-with-Met-9 ray-matching, DCC, Libyan Desert, and **(b only)** SCIAMACHY-with-Met-9 absolute calibration methods **(a)** before and **(b)** after application of the SBAF.

In order to quantify how much of the SBAF-related changes are owed to spectral band adjustments accounting for differential gaseous absorption, the impact of the top-of-atmosphere incoming solar flux differences must be known. Spectral corrections based on radiance, rather than on reflectance, are used in practice because, when working in a radiance framework, band-specific solar flux discrepancies are intrinsically accounted for. This study uses the MODIS Characterization Support Team (MCST) incoming solar spectra, and after weighting by the SRFs, the computed band solar constants are 509.34 $Wm^{-2}sr^{-1}\mu m^{-1}$ and 516.17 $Wm^{-2}sr^{-1}\mu m^{-1}$ for the Aqua-MODIS CH1 and Met-9 CH1 imagers, respectively. For the Met-9 HRV channel, the computed solar constant is 449.68 $Wm^{-2}sr^{-1}\mu m^{-1}$. The ratio of the MCST solar constants (SCs) for Met-9 CH1 (HRV) to Aqua-MODIS CH1 is 1.013 (0.883). Table 1 details, for both the CH1 and HRV cases, the expected gains if only a correction for the SC difference is applied, compared to gains found after an SBAF is applied. The expected SC-dependent-only gains are found by multiplying the pre-SBAF gains by the appropriate SC ratio. The change from applying the SC ratio is rather uniform across the different scene types, averaging at +1.3% and -11.7% for the CH1 and HRV analyses, respectively. When considering narrowband-to-broadband gaseous absorption discrepancies, the desert case requires a -4.5% correction, according to Table 1, whereas the DCC case requires a +3.2% correction – a difference of nearly 8%. For the similar narrowband channels, the correction from the absorption discrepancies is +0.5% and +1.1%, for DCC and desert, respectively. In the CH1 case, the absorption considerations complement the changes made by SC differences for all methods, whereas in the HRV case, the influence of the SC differences counteracts the changes made by absorption considerations for all but the Libyan Desert technique (see Table 1). As anticipated from Section 3.1, the after-SBAF DCC gains are larger than their SC-corrected counterparts, whereas the after-SBAF desert gains are much lower than the SC-corrected gains. This effect points toward stronger water vapor absorption in the atmosphere over the desert than in the other examined regions, resulting in lower gains than when only SC differences are evaluated.

Table 1. Mean gains ($Wm^{-2}sr^{-1}\mu m^{-1}$ / count) for the CH1 and HRV analyses for before the SBAF application, using only a solar constant (SC) ratio correction, and after the SBAF application.

	Average Gain (CH1) Before SBAF	**Average Gain x SC ratio (CH1)**	**Average Gain (CH1) After SBAF**	**Average Gain (HRV) Before SBAF**	**Average Gain x SC ratio (HRV)**	**Average Gain (HRV) After SBAF**
Terra-MODIS	0.540	0.547	0.551	0.633	0.559	0.566
Aqua-MODIS	0.539	0.546	0.551	0.619	0.547	0.563
DCC	0.541	0.548	0.551	0.631	0.557	0.575
Libya	0.539	0.546	0.552	0.675	0.596	0.569

4. CONCLUSIONS

The effectiveness of using SCIAMACHY-based spectral radiance corrections for improving the calibration of a GEOsat through three independent absolute calibration techniques (Aqua-MODIS-with-Met-9 ray-matching, deep-convective-cloud, and Libyan Desert) was presented. Spectral band difference corrections are necessary to account for inter-band discrepancies in atmospheric absorption and solar flux. These corrections are represented by a regression of SCIAMACHY radiance values that are convolved with the spectral response functions (SRFs) of the Met-9 and Aqua-MODIS instruments, and are applied to Aqua-MODIS radiances to arrive at the predicted radiances for Met-9. Furthermore, the corrections can be engineered to represent specific scene-types, e.g., deep convective or marine stratus clouds, or account for seasonal dependencies. After application of the spectral band adjustment factors (SBAFs), agreement between the three calibration methods is within 0.2% – 1.0%, with similar trends, for both the narrowband-to-narrowband and narrowband-to-broadband corrections. This is an improvement of more than 7% for the HRV channel analysis. Gains from ray-matched comparisons of Met-9 visible counts and SCIAMACHY radiances, with the latter instrument being shown as stable throughout its lifetime, validate the accuracy of the adjustment factors by being within 0.2% – 1.3% of the gains found using the three independent absolute calibration techniques, which all require application of an SBAF.

The SBAFs account for disparate solar flux and gaseous absorption owed to the different SRFs. Intuitively, the variation of the SBAF influence as a function of scene type is greater for the narrowband-to-broadband case than for the

narrowband-to-narrowband case. When considering inter-band gaseous absorption discrepancies, the desert case requires a -4.5% correction, whereas the deep-convective-cloud (DCC) case entails a +3.2% correction. This is a range of almost 8%, implying that the SBAF is rather important in deriving a gain. The reason for the large variation is due to water vapor absorption in the near-IR, which is significant in the atmospheric column above a desert, but not as significant above the tropopause-level DCC tops. For the similar narrowband channels, the correction from the absorption discrepancies is +0.5% and +1.1%, for DCC and desert, respectively, resulting in an SBAF range of 0.6% between scene types. These findings make sense given that the narrow, CH1 bands are similarly shaped, and thus there would be less differential absorption between the instruments. The broader HRV band, however, allows more differential absorption, especially over the desert where there are strong seasonal variations in atmospheric water vapor content. The corrections owed to consideration of the solar constant differences are not disparate for different scene types as they are for absorption correction considerations, but they are more significant in both the CH1 and HRV cases at +1.3% and -11.7%, respectively, on average. The overall improvements gained from these SCIAMACHY-based spectral band difference corrections are valuable in obtaining accurate and consistent absolute calibration among multiple independent inter-calibration techniques.

ACKNOWLEDGMENTS

This research was supported by the NASA Modeling, Analysis, and Prediction Program and the NASA Satellite Calibration Interconsistency Program.

REFERENCES

[1] Tobin, D. C., Revercomb, H. E., Moeller, C. C., and Pagano, T. S., "Use of Atmospheric Infrared Sounder high-spectral resolution spectra to assess the calibration of Moderate resolution Imaging Spectroradiameter on EOS Aqua," J. Geophysical Res. 111, D09S05, (2006).

[2] Wu, X., and Yu, F., "GSICS Algorithm Theoretical Basis Document (ATBD) for GOES-AIRS/IASI Inter-Calibration," Draft version dated 2009, available: https://gsics.nesdis.noaa.gov/wiki/GPRC/AtbdCentral.

[3] Gunshor, M. M., Schmit, T. J., Menzel, W. P., and Tobin, D. C., "Intercalibrations of broadband geostationary imagers using AIRS," J. Atmos. And Oceanic. Technol. 26(4), 746-758, (2009).

[4] Wang, L., Wu, X., Goldberg, M., Cao, C., Li, Y., and Sohn, S.-H., "Comparison of AIRS and IASI radiances using GOES imagers as transfer radiometers toward climate data records," J. Appl. Meteor. Climatol. 49(3), 478-492, (2010).

[5] Goldberg, M., Ohring, G., Butler, J., Cao, C., Datla, R., Doelling, D., Gärtner, V., Hewison, T., Iacovazzi, B., Kim, D., Kurino, T., Lafeuille, J., Minnis, P., Renaut, D., Schmetz, J., Tobin, D., Wang, L., Weng, F., Wu, X., Yu, F., Zhang, P., Zhu, T., "The Global Space-based Inter-Calibration System (GSICS)," Bull. Amer. Meteor. Soc. 92(4), 467-475, (2011).

[6] Bovensmann, H., Burrrows, J. P., Buchwitz, M., Frerick, J., Noël, S., Rozanov, V. V., Chance, K. V., and Goede, A. P. H., "SCIAMACHY: Mission objectives and measurement modes," J. Atmos. Sci. 56, 127-150, (1999).

[7] Skupin, J., Noël, S., Wuttke, M. W., Gottwald, M., Bovensmann, H., Weber, M., and Burrows, J. P., "SCIAMACHY Solar Irradiance Observation in the Spectral Range from 240 to 2380 nm," Adv. Space Res. 35, 370-375 (2005).

[8] Lichtenberg, G., et al., "SCIAMACHY Level 1 data: calibration concept and in-flight calibration," Atmos. Chem. Phys. 6, 5347-5367 (2006).

[9] Disclaimer for SCIAMACHY IPF 7.03 Level 1b products (SCI_NL__1P) PO-RSMDA-GS-2009 Volume 15 Issue 3L, (2011).

[10] Doelling, D. R., Lukashin, C., Minnis, P., Scarino, B., and Morstad, D., "Spectral reflectance corrections for satellite intercalibrations using SCIAMACHY data," IEEE Geosci. Remote Sens. Lett. 9(1), 119-123 (2012).

[11] Minnis, P. and Sun-Mack, S., et al., "CERES edition-2 cloud property retrievals using TRMM VIRS and terra and aqua MODIS data, Part I: Algorithms," IEEE Trans. Geosci. Remote Sens. 49, (2011).

[12] Bhatt, R., Doelling, D. R., Morstad, D. L., Scarino, B. R., and Gopalan, A., "Desert-based absolute calibration of successive geostationary visible sensors using a daily TOA radiance model," Submitted IEEE Transactions on Geoscience and Remote Sensing, TGRS-2012-00253 (2012).

[13] Morstad, D. L., Doelling, D. R., Bhatt, R., and Scarino, B., "The CERES calibration strategy of the geostationary visible channels for CERES cloud and flux products," Proc. SPIE 8153, 815316-815316-13 (2011).
[14] Bhatt, R., Doelling, D. R., Scarino, B. R., Morstad, D. L., "Desert based absolute calibration of visible sensors," Proc. IGARSS, 3982 (2012).
[15] Minnis, P., L. Nguyen, D. R. Doelling, D. F. Young, W. F. Miller, "Rapid calibration of operational and research meteorological satellite imagers, Part I: Use of the TRMM VIRS or ERS-2 ATSR-2 as a reference," J. Atmos. Ocean. Technol. 19, 1233-1249, (2002).
[16] Doelling, D., Bhatt, R., Morstad, D., Scarino, B., "Algorithm theoretical basis document for ray-matching technique of calibrating GEO sensors with Aqua-MODIS for GSICS," NASA Langley Research Center, (2011).
[17] Doelling, D. R., Scarino, B. R., Morstad, D., Gopalan, A., Lukashin, C., and Minnis, P., "The calibration of geostationary visible imagers using operational hyper-spectral SCIAMACHY radiances," Submitted IEEE Transactions on Geoscience and Remote Sensing, TGRS-2012-00257 (2012).
[18] Doelling, D. R., Morstad, D. L., Scarino, B. R., Bhatt, R., and Gopalan, A., "The characterization of deep convective clouds as an invariant calibration target and as a visible calibration technique," Submitted IEEE Transactions on Geoscience and Remote Sensing, TGRS-2012-00254 (2012).
[19] Doelling, D., Morstad, D., Bhatt, R., Scarino, B., "Algorithm Theoretical Basis Document for Deep Convective Cloud technique of calibrating GEO sensors with Aqua-MODIS for GSICS," NASA Langley Research Center, (2011).
[20] Hu, Y., B. Wielicki, P. Yang, P. Stackhouse, B. Lin, and D. Young, "Application of deep convective cloud albedo observations to satellite-based study of terrestrial atmosphere: monitoring stability of space-borne measurements and assessing absorption anomaly," IEEE Trans. Geosci. Remote Sens. 42(11), 2594-2599, (2004).
[21] Wu, A., Xiong, X., Doelling, D. R., Morstad, D. L., Angal, A., and Bhatt, R., "Characterization of Terra and Aqua MODIS VIS, NIR, and SWIR spectral band calibration stability," IEEE Trans. on Geosci. Remote Sen., submitted Nov. 28 (2011).
[22] Xiong, X., Sun, J., Wu, A., Chiang, K. Esposito, J., and Barnes, W., "Terra and Aqua MODIS calibration algorithms and uncertainty analysis, Sensors, Systems, and Next-Generation Satellites IX," Proc. SPIE 5978, 59780V (2005).